VENTURINI, G., STEINMETZ, J. & ROQUES, B. (1982). *J. Less-Common Met.* **87**, 21-30.

YARMOLYUK, YA, P., KOTUR, B. YA. & GRIN, YU. N. (1980). *Dopov. Akad. Nauk Ukr. RSR, Ser. B*(11), pp. 68-72.

YARMOLYUK, YA. P., SIKIRITSA, M., AKSELRUD, L. G., LYSENKO, L. A. & GLADYSHEVSKII, E. I. (1982). *Sov. Phys. Crystallogr.* **27**, 1090-1093.

YVON, K., JEITSCHKO, W. & PARTHÉ, E. (1977). *J. Appl. Cryst.* **10**, 73-74.

Acta Cryst. (1985). B**41**, 219-225

Electron-Microscopic Study of the Structure of Metastable Oxides Formed in the Initial Stage of Copper Oxidation. III. $Cu_{64}O$

BY R. GUAN

Institute of Metal Research, Academia Sinica, Shenyang, People's Republic of China

H. HASHIMOTO

Department of Applied Physics, Osaka University, 2-1 Yamadaoka, Suita, Osaka 565, Japan

AND K. H. KUO

Institute of Metal Research, Academia Sinica, Shenyang, People's Republic of China

(*Received 5 October* 1984; *accepted 19 December* 1984)

Abstract

Besides Cu_4O and Cu_8O reported previously, a third metastable copper oxide with the chemical composition $Cu_{64}O$ formed in the early stage of oxidation of copper has been observed by high-resolution electron microscopy. The atomic positions of Cu and O have been determined by electron diffraction and by comparison of the observed structure images with simulated ones calculated on the basis of the dynamical theory of electron diffraction and image formation theory. $Cu_{64}O$ is ordered base-centered orthorhombic with lattice constants $a = 9{\cdot}74$, $b = 10{\cdot}58$ and $c = 16{\cdot}20$ Å. The intensity of the diffracted waves reflecting the periodicity of the O-atom arrangement in $Cu_{64}O$ is much weaker than those in Cu_4O and Cu_8O because of the lower oxygen content. Thus, the images of O atoms in the $Cu_{64}O$ crystal can only be observed at limited thicknesses. Good agreement between the observed and calculated images has been obtained, though the distance between the Cu atoms in $Cu_{64}O$ is still too small to be resolved.

1. Introduction

The contributions made by high-resolution electron microscopy (HREM) to the understanding of the early stages of copper oxidation by the present authors (Guan, Hashimoto & Yoshida, 1984; Guan, Hashimoto & Kuo, 1984) have shown that two suboxides, Cu_4O and Cu_8O, are formed as the interstitial solution of O atoms in the Cu lattice. These results strongly suggest that a series of copper suboxides containing much less oxygen than the normal ones, such as CuO and Cu_2O, might form. Suboxides in b.c.c. transition metals have been studied by several workers, but recently Dahmen & Thomas (1979) showed that previously published results claiming the $Ta_{64}C$ ordered phase are incorrect and can be explained completely in terms of oxygen contamination yielding the compound $Ta_{12}O$.

Khachaturyan (1983) has presented theoretical criteria based on elastic strain energy to predict site occupancy and ordered structures in b.c.c. transition-metal dilute solutions with C, N, O, *etc.* but similar problems concerning the interstitials in f.c.c. metals such as Cu have not been considered. In the present paper, which is the third in the series, the structure of a suboxide phase has been determined to be $Cu_{64}O$ by high-resolution structure imaging and electron diffraction.

2. Specimen preparation and observation

$Cu_{64}O$ was found in pure commercial copper powder, similarly to the case of Cu_8O. It could also be obtained by gently heating copper powder in air. Details of specimen preparation were presented in the previous paper (Guan, Hashimoto & Kuo, 1984). Electron-microscopic observations were made using a JEM 200CX electron microscope. Fig. 1 shows electron micrographs of the new suboxide of copper which, for convenience, is designated as Cu_zO. Fig. 1(*a*) is obtained from pure copper powder, while Fig. 1(*b*) is from the powder heated in air. Electron diffrac-

0108-7681/85/040219-07$01.50

tion patterns from these two types of powders are shown in Figs. 2(*a*) and 3(*a*), respectively. The electron diffraction pattern of Cu_8O in the [010] orientation and a schematic diffraction pattern in the [001] orientation are shown in Figs. 2(*b*) and 3(*b*) for comparison. Figs. 2(*c*) and 3(*c*) are the superimposed diagrams of Figs. 2(*a*) and 2(*b*) and Figs. 3(*a*) and 3(*b*) respectively in which the small differences in the lattice parameters between Cu_2O and Cu_8O have been neglected. In Figs. 2(*c*) and 3(*c*), the circles represent the electron diffraction spots of Cu_8O, while the black dots represent those of Cu_2O. HREM images of Cu_2O with a direct magnification of about 10^6 are shown in Figs. 4 and 5, the corresponding electron diffraction pattern is Fig. 3(*a*). In Fig. 4 a number of regions marked *A* to *C* show different image contrasts. In Fig. 5(*a*), the image is simple and the spacing between the bright spots is quite large, while in (*b*) the image is complex and the spacing smaller. However, both images are from the same crystallite.

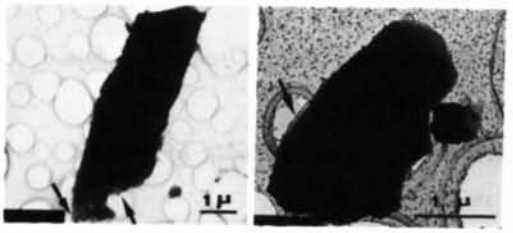

(*a*) (*b*)

Fig. 1. (*a*) Electron micrograph of a thin Cu_2O crystal formed at the edge of a copper powder stored at room temperature in contact with air for more than 20 years. (*b*) Electron micrograph of a Cu_2O crystal formed by heating copper powder in air.

3. Crystal structure

From the similarity with the results obtained in the previous investigations (Guan, Hashimoto & Yoshida, 1984; Guan, Hashimoto & Kuo, 1984), it can be assumed that Cu_2O grows epitaxially on the surface of copper crystals. Furthermore, it can be supposed that O atoms, appearing as bright spots in the structure images, are situated in the distorted tetrahedra comprising Cu atoms.

By comparing the electron diffraction patterns of Cu_8O with those of Cu_2O, shown in Figs. 2(*a*,*b*) and 3(*a*,*b*), it is clear that all the diffraction spots of Cu_8O are present in Cu_2O, but the latter has more spots than the former and the basic period of Cu_2O is about twice as large as that of Cu_8O. However, it can be seen in Fig. 6 that the diffraction spots of pure copper do not match exactly with those of Cu_2O and this mismatch is measured from the diffraction pattern as 13% in the [001] direction of copper. In a schematic drawing of superposition of diffraction patterns of copper and Cu_2O in the [001] orientation shown in

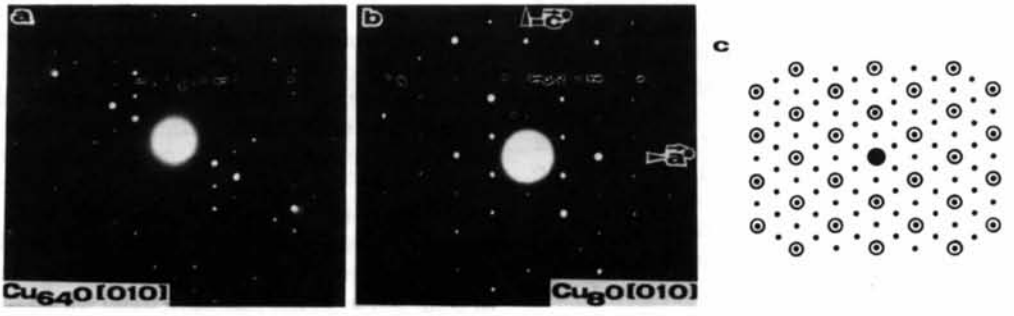

Fig. 2. (*a*) Electron diffraction pattern of the crystal shown in Fig. 1(*b*). (*b*) Electron diffraction patterns of Cu_8O [010]. (*c*) Superposed diagram of (*a*) and (*b*).

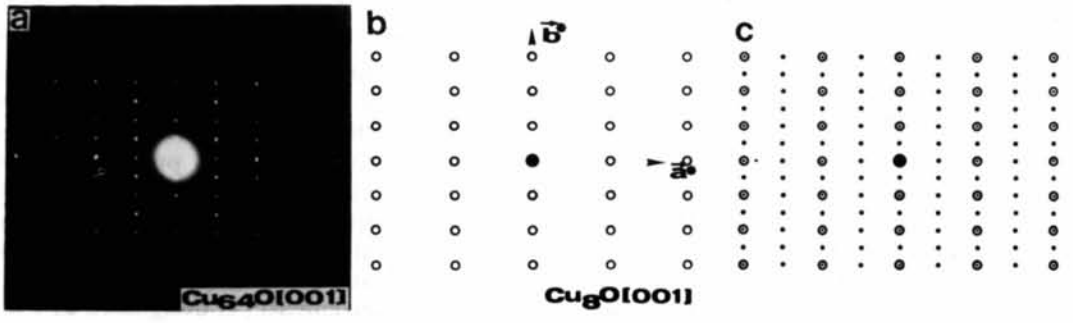

Fig. 3. (*a*) Electron diffraction pattern of the crystal shown in Fig. 1(*a*). (*b*) Schematic diagram of electron diffraction pattern of Cu_8O [001]. (*c*) Superposed diagram of (*a*) and (*b*).

Figs. 7(*a*) and 7(*b*) respectively, one can see that the reciprocal basic vectors **a*** and **b*** of copper are rotated by 45° with respect to those of Cu_xO. The large black dots *A*, *B* and *C* in this figure represent the diffraction spots 200, 020 and 220 of pure copper, respectively, while the small ones *A'*, *B'* and *C'* are the nearest spots from those of Cu_xO. It is clear that the lattice of matrix copper is distorted by the inclusion of interstitial atoms and the angle between the lattice *a* and *b* of the unit cell of copper in the Cu_xO crystal is about 85°.

Based on such a comparison of the electron diffraction patterns between Cu_xO and Cu_8O, a two-dimensional structure model of Cu_xO in the [010] orientation can be obtained by removing every second array of O atoms in the model of Cu_8O as shown in Fig. 8. In this model, the black spots represent Cu atoms. But as shown in Fig. 6(*b*) the *c* axis of the Cu unit cell in Cu_xO is larger than that of pure copper by about 13%.

Similarly, another two-dimensional structure model of Cu_xO in the [001] orientation was also obtained as shown in Fig. 9. The unit cell of copper matrix Cu is outlined by thin lines in the same figure.

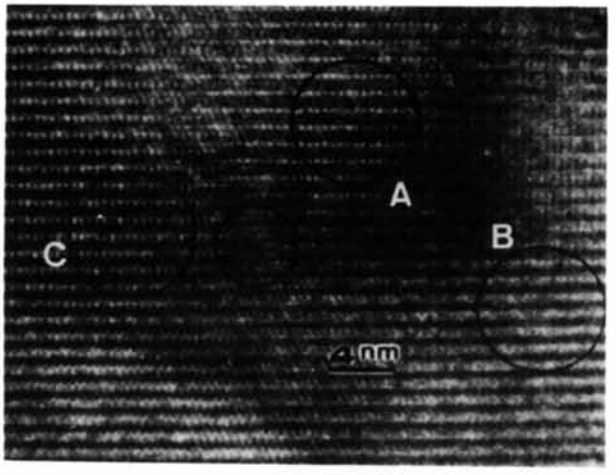

Fig. 4 A highly magnified image of the Cu_xO crystal shown in Fig. 1(*a*). Direct magnification is 8×10^5 times. Areas marked by *A*, *B* and *C* are discussed in Figs. 5 and 17.

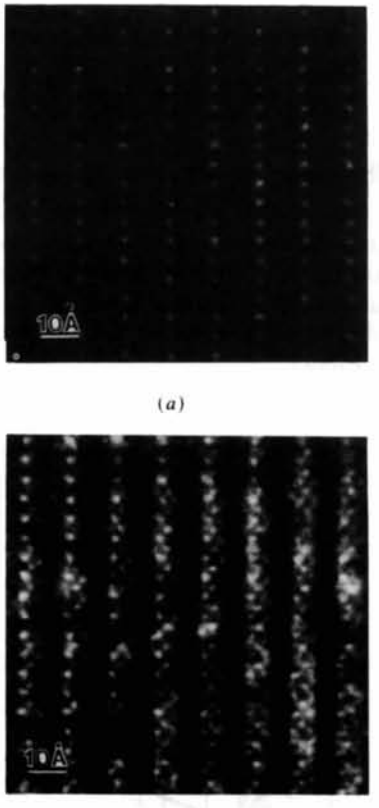

Fig. 5. (*a*) The magnified image taken from the encircled area *A* of Fig. 4. (*b*) The magnified image taken from the encircled area *B* of Fig. 4.

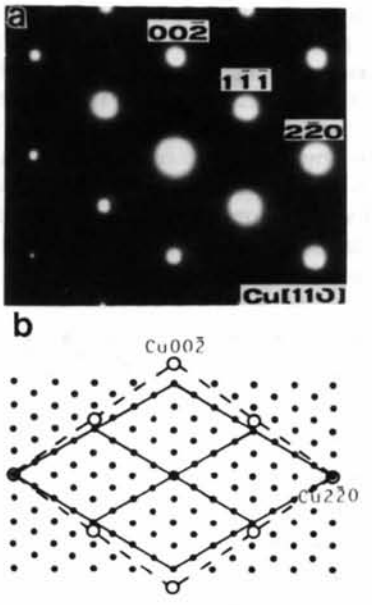

Fig. 6. (*a*) Electron diffraction pattern of copper in [110] orientation. (*b*) Superposed diagram of the electron diffraction patterns shown in Figs. 2(*a*) (●) and 6(*a*) (○).

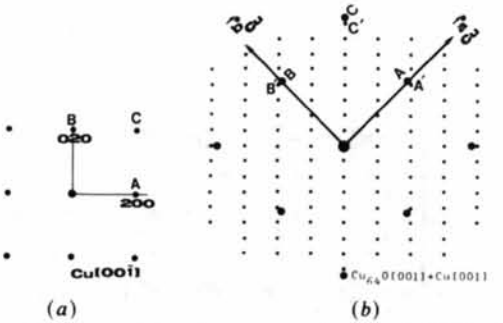

Fig. 7. (*a*) Electron diffraction pattern of copper in [001] orientation. (*b*) Superposed diagram of the electron diffraction patterns shown in Figs. 3(*a*) (●) and 7(*a*) (○).

But as shown in Fig. 7(*b*) the basic vectors **a** and **b** of the unit cell of copper are not exactly perpendicular to each other, but have an angle of 85° between them. Based on these two-dimensional structure models, a three-dimensional structure model of Cu_zO was constructed as shown in Fig. 10. This is base-centered orthorhombic with $a=9{\cdot}74$, $b=10{\cdot}58$ and $c=16{\cdot}20$ Å and belongs to the space group *Bmm*2. The atom positions are given in Table 1 with the coordinate changes of *abc* (*Amm*2) into *bac̄* (*Bmm*2) (Hahn, 1983). From this, it is clear that the structure is an interstitial ordered solid solution of O in Cu.

The structural relationship between Cu_zO and Cu is shown in Fig. 10 with the origin of the coordinates chosen at the position of an O atom. The unit cell of Cu_zO is outlined by thick lines and that of copper by thin lines. Evidently, each unit cell of Cu_zO contains 32 unit cells of Cu and the ratio of O to Cu is 1:64. Therefore its chemical formula can be designated as $Cu_{64}O$.

To confirm the structure model, four electron diffraction patterns from this compound are indexed on the basis of $Cu_{64}O$ as shown in Fig. 11. The reciprocal-lattice vector **g** and the angles obtained from the observed diffraction patterns are shown in Table 2 for four different orientations and are compared with the calculated ones. It is seen that the calculated values from the model agree very well with the experimentally observed ones, showing that the proposed model is correct.

Table 1. *Atomic positions of* Cu *and* O *atoms in the unit cell of* $Cu_{64}O$; *space group Bmm*2

Element	Multiplicity, Wyckoff letter	Coordinates of equivalent positions $(0,0,0;\frac{1}{2},0,\frac{1}{2})+$	x, y, z
Cu	$8f_1$	$x,y,\bar{z};\bar{x},\bar{y},\bar{z};\bar{x},y,\bar{z};x,\bar{y},\bar{z}$	$x=\frac{1}{8}, y=\frac{2}{8}, z=\frac{3}{16}$
Cu	$8f_2$	$x,y,\bar{z};\bar{x},\bar{y},\bar{z};\bar{x},y,\bar{z};x,\bar{y},\bar{z}$	$x=\frac{1}{8}, y=\frac{2}{8}, z=\frac{7}{16}$
Cu	$8f_3$	$x,y,\bar{z};\bar{x},\bar{y},\bar{z};\bar{x},y,\bar{z};x,\bar{y},\bar{z}$	$x=\frac{1}{8}, y=\frac{2}{8}, z=\frac{11}{16}$
Cu	$8f_4$	$x,y,\bar{z};\bar{x},\bar{y},\bar{z};\bar{x},y,\bar{z};x,\bar{y},\bar{z}$	$x=\frac{1}{8}, y=\frac{2}{8}, z=\frac{15}{16}$
Cu	$8f_5$	$x,y,\bar{z};\bar{x},\bar{y},\bar{z};\bar{x},y,\bar{z};x,\bar{y},\bar{z}$	$x=\frac{2}{8}, y=\frac{1}{8}, z=\frac{13}{16}$
Cu	$8f_6$	$x,y,\bar{z};\bar{x},\bar{y},\bar{z};\bar{x},y,\bar{z};x,\bar{y},\bar{z}$	$x=\frac{2}{8}, y=\frac{1}{8}, z=\frac{9}{16}$
Cu	$8f_7$	$x,y,\bar{z};\bar{x},\bar{y},\bar{z};\bar{x},y,\bar{z};x,\bar{y},\bar{z}$	$x=\frac{2}{8}, y=\frac{3}{8}, z=\frac{5}{16}$
Cu	$8f_8$	$x,y,\bar{z};\bar{x},\bar{y},\bar{z};\bar{x},y,\bar{z};x,\bar{y},\bar{z}$	$x=\frac{2}{8}, y=\frac{1}{8}, z=\frac{1}{16}$
Cu	$8f_9$	$x,y,\bar{z};\bar{x},\bar{y},\bar{z};\bar{x},y,\bar{z};x,\bar{y},\bar{z}$	$x=\frac{2}{8}, y=\frac{3}{8}, z=\frac{13}{16}$
Cu	$8f_{10}$	$x,y,\bar{z};\bar{x},\bar{y},\bar{z};\bar{x},y,\bar{z};x,\bar{y},\bar{z}$	$x=\frac{2}{8}, y=\frac{3}{8}, z=\frac{9}{16}$
Cu	$8f_{11}$	$x,y,\bar{z};\bar{x},\bar{y},\bar{z};\bar{x},y,\bar{z};x,\bar{y},\bar{z}$	$x=\frac{2}{8}, y=\frac{3}{8}, z=\frac{5}{16}$
Cu	$8f_{12}$	$x,y,\bar{z};\bar{x},\bar{y},\bar{z};\bar{x},y,\bar{z};x,\bar{y},\bar{z}$	$x=\frac{2}{8}, y=\frac{3}{8}, z=\frac{1}{16}$
Cu	$4e_1$	$x,\frac{1}{2},\bar{z};\bar{x},\frac{1}{2},\bar{z}$	$x=\frac{1}{8}, z=\frac{3}{16}$
Cu	$4e_2$	$x,\frac{1}{2},\bar{z};\bar{x},\frac{1}{2},\bar{z}$	$x=\frac{1}{8}, z=\frac{7}{16}$
Cu	$4e_3$	$x,\frac{1}{2},\bar{z};\bar{x},\frac{1}{2},\bar{z}$	$x=\frac{1}{8}, z=\frac{11}{16}$
Cu	$4e_4$	$x,\frac{1}{2},\bar{z};\bar{x},\frac{1}{2},\bar{z}$	$x=\frac{1}{8}, z=\frac{15}{16}$
Cu	$4d_1$	$x,0,\bar{z};\bar{x},0,\bar{z}$	$x=\frac{1}{8}, z=\frac{3}{16}$
Cu	$4d_2$	$x,0,\bar{z};\bar{x},0,\bar{z}$	$x=\frac{1}{8}, z=\frac{7}{16}$
Cu	$4d_3$	$x,0,\bar{z};\bar{x},0,\bar{z}$	$x=\frac{1}{8}, z=\frac{11}{16}$
Cu	$4d_4$	$x,0,\bar{z};\bar{x},0,\bar{z}$	$x=\frac{1}{8}, z=\frac{15}{16}$
Cu	$4c_1$	$0,y,\bar{z};0,\bar{y},\bar{z}$	$y=\frac{1}{8}, z=\frac{1}{16}$
Cu	$4c_2$	$0,y,\bar{z};0,\bar{y},\bar{z}$	$y=\frac{1}{8}, z=\frac{5}{16}$
Cu	$4c_3$	$0,y,\bar{z};0,\bar{y},\bar{z}$	$\bar{y}=\frac{1}{8}, z=\frac{9}{16}$
Cu	$4c_4$	$0,y,\bar{z};0,\bar{y},\bar{z}$	$y=\frac{1}{8}, z=\frac{13}{16}$
Cu	$4c_5$	$0,y,\bar{z};0,\bar{y},\bar{z}$	$y=\frac{3}{8}, z=\frac{1}{16}$
Cu	$4c_6$	$0,y,\bar{z};0,\bar{y},\bar{z}$	$y=\frac{3}{8}, z=\frac{5}{16}$
Cu	$4c_7$	$0,y,\bar{z};0,\bar{y},\bar{z}$	$y=\frac{3}{8}, z=\frac{9}{16}$
Cu	$4c_8$	$0,y,\bar{z};0,\bar{y},\bar{z}$	$y=\frac{3}{8}, z=\frac{13}{16}$
O	$2a$	$0,0,\bar{z}$	$z=0$

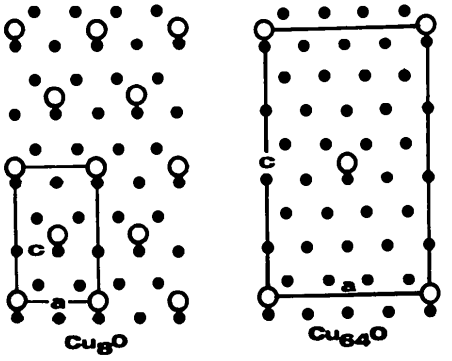

Fig. 8. Projection of Cu (●) and O (○) atoms of the structure model of $Cu_{64}O$ in [010] and Cu_8O in [010]. The unit cell of $Cu_{64}O$ is outlined by thick lines.

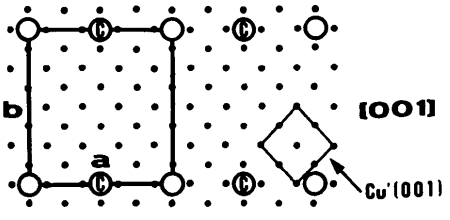

Fig. 9. Projection of Cu (●) and O (○) atoms of the structure model of $Cu_{64}O$ in [001]. The unit cell of $Cu_{64}O$ is outlined by thick lines and that of Cu by thin lines.

4. High-resolution electron microscopy and simulated images

In order to confirm the crystal structure of $Cu_{64}O$, a comparison has been made for the observed images with simulated ones calculated on the basis of the dynamical theory of electron diffraction and image formation theory.

Fig. 12 shows the change of the amplitudes of the main diffracted waves of $Cu_{64}O$ in the [001] orientation with specimen thickness. It can be seen that the amplitudes of the diffracted wave 01 and 20 (representing, for brevity, reflections 010 and 200) which

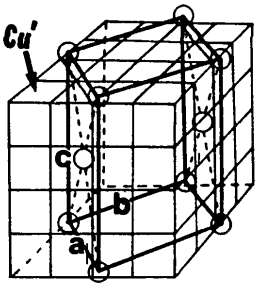

Fig. 10. Orientation relationship between the unit cells of $Cu_{64}O$ (thick lines) and Cu (thin lines). ○: O atom.

Table 2. *Analysis of the electron diffraction patterns shown in Fig.* 11 *with reference to the* $Cu_{64}O$ *crystal structure*

No.	*UVW*	$h_1k_1l_1$	$h_2k_2l_2$	$g_2(h_2k_2l_2)/g_1(h_1k_1l_1)$ Calc.	Obs.	$\Phi(g_1, g_2)$ Calc.	Obs.	$d_1(1/g_1)$ Calc.	Obs.
1	010	$10\bar{1}$	$\bar{1}0\bar{1}$	1·00	1·0	118·0	119·0	8·40	8·6
2	001	010	200	2·16	2·1	90·0	90·0	10·52	10·5
3	210	002	$1\bar{2}1$	1·82	1·8	74·1	73·0	8·13	8·1
4	$20\bar{3}$	010	604	6·97	6·9	90·0	90·0	10·52	10·4

reflect the periodicity of the O atoms, are rather weak and their amplitudes increase very slowly with increasing specimen thickness, in contrast to the corresponding reflections in Cu_4O (Guan, Hashimoto & Yoshida, 1984) and Cu_8O (Guan, Hashimoto & Kuo, 1984). This is probably due to the very low oxygen content in $Cu_{64}O$. Therefore, the intensity of the diffracted waves contributed by O atoms in $Cu_{64}O$ is very weak and hence only Cu atoms appear in the image at the weak phase object condition, as shown in Fig. 13(*a*). At a thickness of about 260 Å, the amplitudes of the diffracted waves 80 and 08 which reflect the arrangement of Cu atoms become a minimum, while the amplitude of the wave 01 is larger than those of 44 and 08 to make only O atoms appear in Fig. 13(*b*). In Fig. 13(*c*), a clear O-atom image and very faint Cu-atom images appear because the wave 01 is still quite strong. The faint contrast near the images of the O atom will be discussed later. The image shown in Fig. 5(*a*) was obtained at a thickness corresponding to Fig. 13(*b*) and thus only O atoms are imaged. Fig. 14 shows a comparison of the mag-

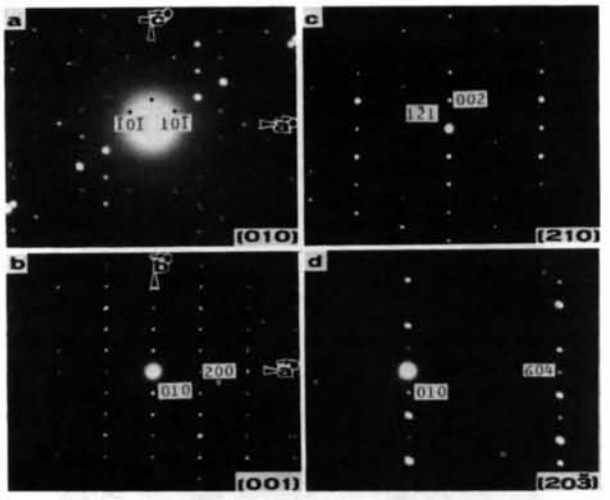

Fig. 11. Electron diffraction patterns of $Cu_{64}O$ in four different orientations. Indices are based on the orthorhombic unit cell shown in Fig. 10.

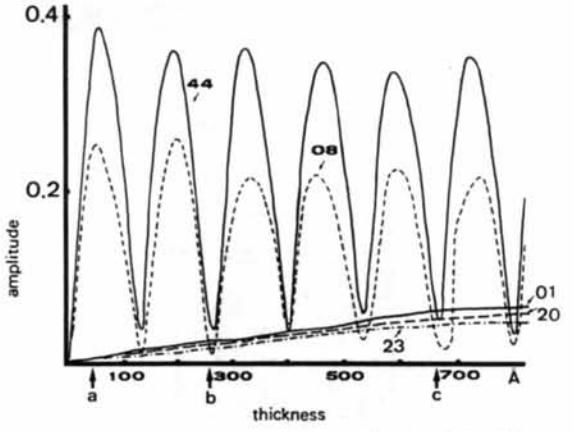

Fig. 12. Thickness dependence of the amplitudes of the diffracted waves normalized to the incident wave from several atomic planes of the $Cu_{64}O$ structure in the [001] orientation. For brevity, 010, 200, *etc.* are expressed as 01, 20, *etc.*

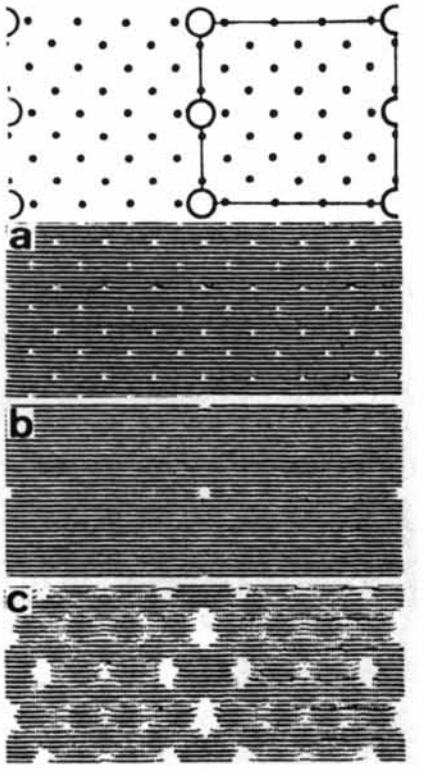

Fig. 13. Calculated images ($\Delta f = C_s = 0$) for thicknesses of (*a*) 49 Å, (*b*) 260 Å and (*c*) 665 Å which correspond to *a*, *b* and *c* respectively in Fig. 12. The uppermost is a model. The excited and contributed waves to the image intensity are within the range of 1·5 $Å^{-1}$.

nified image of Fig. 5(*a*) and simulated images with the structure model at a thickness of 260 Å. It can be seen that the observed bright spots correspond to the positions of O atoms only at the thickness shown by *b* in Fig. 12.

Although the amplitudes of the diffracted waves of 08 and 44, which reflect the arrangement of Cu atoms, are very strong at most of the thicknesses as shown in Fig. 12, the images of the Cu atoms have not been observed up to now because the spacing of the Cu atoms in the suboxides is too small to be resolved ($d_{08} = 1{\cdot}2$, $d_{44} = 1{\cdot}7$ Å). At a thickness of about 665 Å, the intensities of 01, 20 and 23 are higher than those of 44 and 08, those of 01 and 20 being nearly equal to 44, as indicated by the arrow *c* in Fig. 12. This suggests that images relating to such lattice planes should be observed at such a thickness. Fig. 5(*b*) as well as its magnified image in Fig. 15 (top) is probably such an example. In this figure a series of bright bands with the same periodicity as that of O shown in Fig. 14 can be observed. Between them there are a number of bright spots which do not exactly reflect the Cu-atom positions of $Cu_{64}O$ at a thickness of 665 Å, as confirmed by the image simulation (Fig. 15, bottom). The agreement between the observed and simulated images is quite good. Fig. 16 is a schematic diagram of the suggested model for the interpretation of Fig. 15. According to the amplitude-thickness diagram (Fig. 12) and the simulation results, it is suggested that the diffracted waves 01, 20 and 23 constitute the 23 lattice image shown by the dotted lines in Fig. 16. Fig. 13(*c*) is the intensity distribution at the bottom surface of the crystal but shows the main features such as the bright-dark bands. Fig. 17 gives an image of region *C* in Fig. 4 with the corresponding simulated image obtained at the thickness of 670 Å. The good agreement between the observed and calculated images indicates that the proposed structure model of $Cu_{64}O$ is correct.

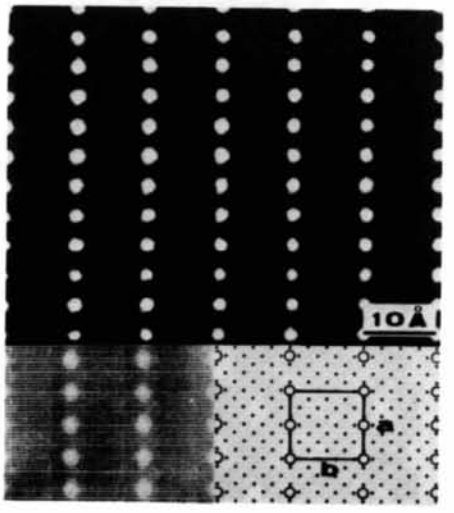

Fig. 14. The calculated image and the structure model of $Cu_{64}O$ with the projection of Cu and O atoms on (001) are shown together with the observed image. Parameters used for the calculation are $t = 130$, 260, 395, 520 Å, $C_s = 1{\cdot}2$ mm, $\Delta f = 300$ Å, where t is the thickness.

5. Discussion

The present investigation has confirmed the existence of a $Cu_{64}O$ phase at the very early stage of oxidation of copper. The distribution of O atoms in $Cu_{64}O$ clearly indicates that they have a tendency to order themselves in the metal lattice forming a regular stable structure, by occupying specific tetrahedral interstitial sites.

Although the conditions for the growth of $Cu_{64}O$ are very similar to those of Cu_8O, the chances of finding $Cu_{64}O$ during electron-microscope observation are much less than that of Cu_8O. The lattice parameters *a*, *b* and *c* of $Cu_{64}O$ are about 1·8 times,

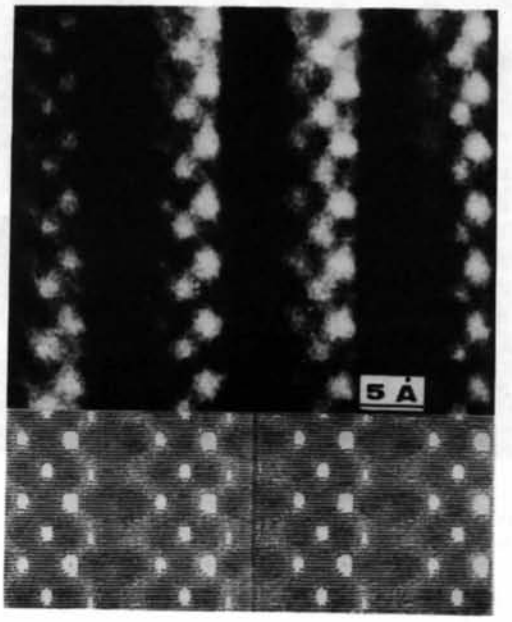

Fig. 15. Comparison between the observed (top) and the simulated (bottom) images. Parameters used for the calculation are $t =$ 665 Å, $C_s = 1{\cdot}2$ mm, $\Delta f = -300$ Å. The projection of the Laue point to (110) is given by $0{\cdot}7g_{100}$, $0{\cdot}3g_{010}$ (deviated from the Bragg condition).

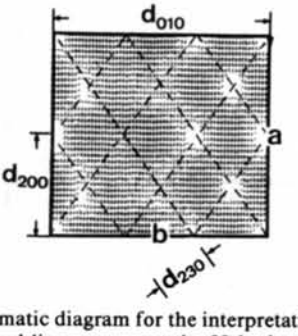

Fig. 16. A schematic diagram for the interpretation of Fig. 15. The dashed lines represent the 23 lattice planes.

instead of two times, larger than those of Cu_8O, which indicates that the expansion of the $Cu_{64}O$ lattice due to the interstitial O atoms in the Cu lattice is less than that in Cu_8O. It is possible that such a strain may cause distortions of the substrate metal and if the strain is large enough it will result in a separation of the 'oxidized' part from the matrix and produce a large number of very small and thin slightly 'oxidized' crystallites. This may be one of the reasons why Cu_8O can be more easily found than $Cu_{64}O$ during observation in the electron microscope. It may be noted that, for the suboxides with very low oxygen content, the structure images cannot be obtained from a very thin crystal, *i.e.* the weak phase object condition, but can be obtained from a thicker specimen in the dynamic scattering object condition. On increasing the thickness of the crystal to more than a certain critical thickness, the contrast of the images of the heavy atoms decreases and that of the light atoms increases. Thus at some optimum thickness of the crystal, the images of the light atoms can be observed as well as those of the heavy atoms. Thus the dynamical scattering of electron waves can be used effectively for the structure analysis of the crystals containing light atoms.

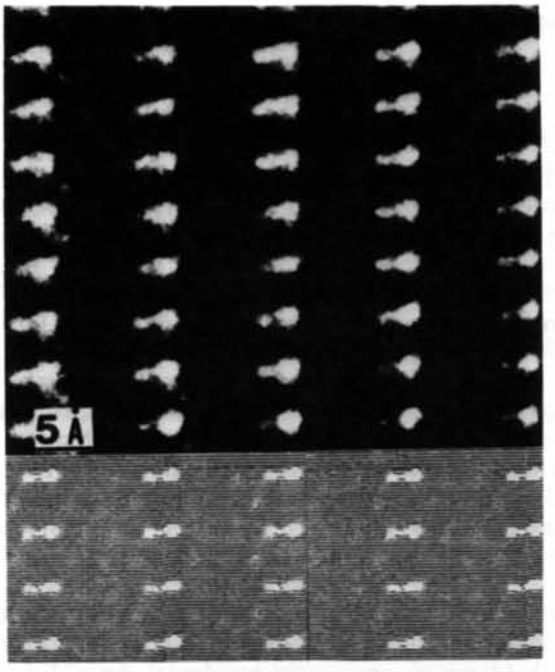

Fig. 17. Comparison of the observed and calculated images of $Cu_{64}O$. The magnified images on the top, taken from the encircled area *C* in Fig. 4, match the calculated ones (bottom) obtained with the value of defocus of $\Delta f = -500$ Å and thickness of $t = 670 \sim 700$ Å.

The authors would like to record their thanks to Mr B. S. Zou and Drs H. Endoh, M. Tomita and N. Ajika for their help in the experiments and to Mr Y. K. Wu, and Professors G. Thomas and S. Suryanarayana for helpful discussions.

References

DAHMEN, U. & THOMAS, G. (1979). *Scr. Metall.* **13**, 527–530.
GUAN, R., HASHIMOTO, H. & KUO, K. H. (1984). *Acta Cryst.* B**40**, 560–566.
GUAN, R., HASHIMOTO, H. & YOSHIDA, T. (1984). *Acta Cryst.* B**40**, 109–114.
HAHN, T. (1983). Editor. *International Tables for Crystallography*, Vol. *A*, pp. 56–57, 234–235.
KHACHATURYAN, A. G. (1983). *Theory of Structural Transformations in Solids.* New York: John Wiley.

Acta Cryst. (1985). B**41**, 225–230

A Combined X-ray and Neutron Diffraction Study of Bi_3ReO_8; a New Structure Type Based on Fluorite

BY A. K. CHEETHAM* AND A. R. RAE SMITH

Department of Chemical Crystallography, University of Oxford, 9 Parks Road, Oxford OX1 3PD, England

(*Received* 21 *October* 1984; *accepted* 6 *February* 1985)

Abstract

The fluorite-related crystal structure of Bi_3ReO_8 has been solved by a combination of X-ray and neutron diffraction techniques. The lattice is cubic, $a = 11{\cdot}590\,(1)$ Å, space group $P2_13$, $Z = 8$. The final *R* factors from the neutron powder study were $R_I = 5{\cdot}3\%$, $R_P = 10{\cdot}4\%$. The principal deviation from the ideal fluorite structure is found in the ReO_4 tetrahedra, which are rotated 40° about the ⟨111⟩ direction in order to accommodate the stereochemical activity of the Bi lone pairs. The relationship of the structure to those of the related rare-earth compounds, Ln_3ReO_8, is discussed.

* Author to whom correspondence should be addressed.

0108-7681/85/040225-06$01.50